Colony stimulating factor 1 receptor (Csf1r) expressing cell ablation in mafia (macrophage-specific Fas-induced apoptosis) mice alters monocyte landscape and atherosclerotic lesion characteristics

Medina Rodriguez, Indira; Wieland, E.B.; Temmerman, L.; Otten, J.J.T.; Bermudez, B.; Bot, I.; ... ; Biessen, E.A.L.

European Journal of Immunology
Clinical·Basic·Translational

Innate immunity

Basic

Research Article

Colony stimulating factor 1 receptor (*Csf1r*) expressing cell ablation in mafia (macrophage-specific Fas-induced apoptosis) mice alters monocyte landscape and atherosclerotic lesion characteristics

Indira Medina[1,2], Elias B Wieland[1], Lieve Temmerman[1], Jeroen J.T. Otten[1], Beatriz Bermudez[1], Ilze Bot[2], Timo Rademakers[3], Erwin Wijnands[4], Leon Schurgers[5], Barend Mees[6], Theo J.C. van Berkel[2], Pieter Goossens[##1] and Erik A.L. Biessen[##1,7]

[1] Department of Pathology, Cardiovascular Research Institute Maastricht (CARIM), Maastricht University, Maastricht, the Netherlands
[2] Division of Biopharmaceutics, Leiden Academic Center for Drug Research, Leiden, the Netherlands
[3] MERLN Institute for Technology-Inspired Regenerative Medicine, Maastricht University, Maastricht, the Netherlands
[4] Central Diagnostic Laboratory, Maastricht University Medical Center, Maastricht, the Netherlands
[5] Department of Biochemistry, Maastricht University, Maastricht, the Netherlands
[6] Department of Vascular Surgery, Maastricht University Medical Center, Maastricht, the Netherlands
[7] Institute for Molecular Cardiovascular Research (IMCAR), RWTH Aachen University, Aachen, Germany

Macrophage infiltration and accumulation in the atherosclerotic lesion are associated with plaque progression and instability. Depletion of macrophages from the lesion might provide valuable insights into plaque stabilization processes. Therefore, we assessed the effects of systemic and local macrophage depletion on atherogenesis. To deplete monocytes/macrophages we used atherosclerosis-susceptible *Apoe*$^{-/-}$ mice, bearing a MaFIA (macrophage-Fas-induced-apoptosis) suicide construct under control of the *Csf1r* (CD115) promotor, where selective apoptosis of Csf1r-expressing cells was induced in a controlled manner, by administration of a drug, AP20187. Systemic induction of apoptosis resulted in a decrease in lesion macrophages and smooth-muscle cells. Plaque size and necrotic core size remained unaffected. Two weeks after the systemic depletion of macrophages, we observed a replenishment of the myeloid compartment. Myelopoiesis was modulated resulting in an expansion of CSF1R^{lo} myeloid cells in the circulation and a shift from Ly6c^{hi} monocytes toward Ly6c^{int} and Ly6c^{lo} populations in the spleen. Local apoptosis induction led to a decrease in plaque burden and macrophage content with marginal effects on the circulating myeloid cells. Local, but not systemic depletion of *Csf1r*$^{+}$ myeloid cells resulted in decreased plaque burden. Systemic depletion led to CSF1R^{lo}-monocyte expansion in blood, possibly explaining the lack of effects on plaque development.

Keywords: Apoptosis · Atherogenesis · Atherosclerosis · Cardiovascular immunology · Cardiovascular inflammation · Colony stimulating factor 1 · Csf1r · Inflammation · Innate immunity · Macrophages · Macrophage-specific Fas-induced apoptosis · MaFIA · Monocytes · Monocyte infiltration · Myeloid cell depletion

Additional supporting information may be found online in the Supporting Information section at the end of the article.

Correspondence: Prof. Erik A.L. Biessen
e-mail: erik.biessen@mumc.nl

Indira Medina and Elias Wieland contributed equally to the work.
[##]These authors shared the last authorship.

Introduction

Macrophage accumulation in the atherosclerotic lesion is often considered essential for plaque progression and destabilization. Circulating monocytes are attracted to the lesion site and subsequently differentiate into macrophages mainly in response to CSF-1 (macrophage colony-stimulating factor [M-CSF]) and other cytokines in the subendothelial space. These macrophages take up the accumulated modified lipoproteins, such as oxidized-LDL, via scavenger receptor-mediated phagocytosis and transition to a foamy phenotype. In turn, foamy macrophages favor the progression of inflammation and undergo apoptosis or necrosis, contributing to the formation of a necrotic core. In brief, macrophages are thought to be key players in plaque progression and instability [1].

Even though the net contribution of newly recruited monocytes versus local macrophage proliferation to atherogenesis is still under debate, monocytes, and macrophages were seen to play key roles in lesion development throughout all stages of atherosclerosis [2, 3].

Local production of CSF-1, mostly by endothelial and smooth muscle cells, drives the attraction, differentiation, expansion, and survival of macrophages via the interaction with its receptor, CSF1R or CD115 [4–6]. Further, it was shown that the deficiency in CSF-1 leads to increased macrophage apoptosis and an overall reduction in inflammation and plaque burden [7–10]. Overall, these data underline the important role of the CSF-1-CSF1R interaction on macrophage-driven atherosclerosis progression.

While previous studies mainly focused on determining the effects of systemic or local M-CSF deficiency on macrophages in atherosclerosis, the impact of a specific depletion of myeloid cells that express the CSF1 receptor on atherosclerosis has not yet been elucidated.

Here, we studied the effects of transient myeloid-specific cell depletion in the context of atherosclerosis. To this end, we used the macrophage Fas-induced apoptosis (MaFIA) transgenic mice which express a fusion protein of the Fas receptor and a mutant human FK506 binding protein 1A, under the control of the Csf1r promoter. This model allows for the depletion of *Csf1r*-expressing cells, predominantly monocytes and macrophages, in a time-controlled manner via the administration of a small compound, AP20187 [11]. Previous studies using the MaFIA model underlined the important, however, context-dependent, contributions of $CSF1R^+$ myeloid populations to the progression of different disease models [12–14]. To render the MaFIA mice proatherogenic, they were crossed with $Apoe^{-/-}$ mice and fed a Western-type diet [15]. Rapid atherosclerosis development was induced by perivascular collar placement [16].

Materials and methods

CSF1R for human genes

Atherosclerotic plaque samples were collected as previously described [17] after carotid endarterectomy. Plaque segments whose flanking pieces were either classified as unstable (presenting intraplaque hemorrhage, IPH) or stable were used for downstream analysis [17]. Tissue collection was in line with the Dutch Code for Proper Secondary Use of Human Tissue (http://www.fmwv.nl) and the local Medical Ethical Committee (protocol number 16-4-181). A total of 42 samples (16 IPH^- and 26 IPH^+) were successfully profiled. Transcriptomic data were analyzed using the R Bioconductor *lumi* package (v2.38.0) [18]. First, we performed a variance stabilizing transformation, which is incorporated in the *lumi* package [18]. Then, the robust spline normalization algorithm in the *lumi* package was applied to normalize the data. Gene differential expression analysis was performed using the *Limma* R package (v3.42.2) with Benjamini-Hochberg correction [19]. Multiple transcript isoforms were mapped to the same gene based on the HUGO Gene Nomenclature Committee symbols by selecting the highest expressed transcript. For the plaque composition analysis, we measured the plaque, media, cap, necrotic core, hemorrhage, and luminal thrombus area by morphometric analysis of H&E sections. Other histological features were assessed by immunohistochemistry as described by Jin et al. (2021) [17, 20].

Animals

Mice expressing the $MaFIA^{+/+}$; coexpressing GFP and the inducible suicide receptor under control of the endogenous *Csf1r* promotor, *C57BL/6J−Tg(Csf1r−EGFP−NGFR/FKBP1A/TNFRSF6)2Bck/J* $MaFIA^{+/+}$), obtained from the Jackson Laboratories [11], were crossed to the proatherogenic $Apoe^{-/-}$ background for more than 12 generations at the animal breeding facility at the Leiden university to obtain homozygous $Apoe^{-/-MaFIA}$ mice. The MaFIA transgene was inherited according to Mendelian laws as demonstrated by qPCR analysis of gDNA (PureLink Genomic DNA Purification Kit, Invitrogen). Primer sequences were: 5′-CCACATGAAGCAGCAGGACTT-3′ for the forward primer and 5′-GGTGCGCTCCTGGACGTA-3′ for the reverse primer. During all experiments, animals were housed in filter-top cages, and drinking water and food were provided ad libitum. Mice were fed a regular chow diet (RM3; Special Diet Services, Essex) or a Western-type diet (WTD; 0.25% cholesterol; Special Diet Services). Drinking water supplemented with antibiotics (60,000 Units/L Polymixin B Sulfate [Sigma-Aldrich] and 100 mg/L Neomycin [Sigma-Aldrich]) was introduced 2 weeks before the introduction of a Western-type diet. All in vivo studies were

approved by the Leiden University Ethics Committee for animal experiments and performed according to the Dutch government guidelines for animal experiments.

Time-controlled apoptosis induction using AP20187

Lyophilized AP20187 was dissolved in ice-cold pure (100%) ethanol to obtain a 0.455 mM (6.25 mg/mL) stock solution. This stock solution was stored at −20°C until further use. For in vitro experiments, the stock solution was diluted in culture medium to a final concentration of 1–5 μM, with an end concentration of ethanol below 0.5%. For in vivo experiments with intravenous (IV) injections, a solution containing 4% ethanol, 10% poly(ethylene) glycol (PEG) 400, and 1.7% Tween in water, with 1:25 vol/vol dilution of AP20187 stock solution (final concentration 0.25 mg/mL) was prepared. All IV injections were administered within 30 min after the preparation of this solution. The volume to be injected was adjusted according to the body weight of the mouse to obtain a dose of 1 mg/kg bodyweight, with an average of 150 μL injection per mouse. Because a previous study reported mild induction of thrombocytopenia upon AP20187 administration, *Apoe*$^{-/-}$ control animals received solvent containing AP20187 at the same dose as *Apoe*$^{-/-MaFIA}$ mice [21]. For the in vivo experiments in which osmotic minipumps (Alzet) were used, the stock solution was diluted as before; however, the administered dose was 100-fold lower (0.01 mg/kg).

In vivo experiments

IV injection atherosclerosis study

Ten-week-old male *Apoe*$^{-/-MaFIA}$ animals ($n = 14$) and *Apoe*$^{-/-}$ animals ($n = 13$) were placed on a Western-type diet. Two weeks after introducing the WTD, animals received flow-restricting collars around the right and left carotid arteries to induce atherosclerotic plaque formation, as described before [16]. Three weeks later, *Apoe*$^{-/-MaFIA}$ and *Apoe*$^{-/-}$ mice received, every 72 h, an IV injection containing AP20187 to a final dose of 1 mg/kg body weight in the tail vein for 2 weeks. Bodyweight was measured to adjust the dose according to the individual weight of each mouse and to monitor the effect of the treatment. Mice were euthanized with a single intraperitoneal injection of pentobarbital (100 mg/kg) 18 h after the last injection.

Dynamics study

Ten-week-old *Apoe*$^{-/-MaFIA}$ animals ($n = 16$) and *Apoe*$^{-/-}$ animals ($n = 8$) were placed on a Western-type diet for 5 weeks. Subsequently, *Apoe*$^{-/-MaFIA}$ and *Apoe*$^{-/-}$ mice received every 72 h an IV injection containing AP20187 to a final dose of 1 mg/kg body weight in the tail vein for one or 2 weeks ($n = 8$/timepoint). Bodyweight was measured to adjust the dose according to the individual weight of each mouse. Mice were euthanized 18 h after the last injection.

Osmotic minipump atherosclerosis study

Ten-week-old male *Apoe*$^{-/-MaFIA}$ animals ($n = 8$) and *Apoe*$^{-/-}$ animals ($n = 8$) were placed on a Western-type diet. Two weeks after introducing the WTD, animals received flow-restricting collars around the right and left carotid arteries to induce atherosclerotic plaque formation. Three weeks later, an osmotic minipump containing AP20187 with catheters attached to the perivascular site of the carotid artery was placed. Mice were administered AP20187 via the osmotic minipumps continuously at a dose of 0.01 mg/kg for 2 weeks. Upon sacrifice, the integrity and localization of the catheters were verified and animals with (suspected) malfunctions in the catheters or minipumps were excluded from the study.

In vitro macrophage apoptosis assay

Peritoneal macrophages isolated from *Apoe*$^{-/-MaFIA}$ and *Apoe*$^{-/-}$ mice ($n = 5$ per genotype) were cultured for 24 h in RPMI-1640 (Invitrogen) supplemented with 10% fetal calf serum. Subsequently, AP20187 was added to the medium to a final concentration of 4.55 μM and cells were incubated for 18 h. Apoptosis was measured by immunohistochemical staining for cleaved caspase-3 and counterstaining with DAPI. Pictures were made (Leica DMIL fluorescence microscope) and overlays were analyzed with ImageJ Software.

Histology

Carotid arteries from *Apoe*$^{-/-MaFIA}$ and *Apoe*$^{-/-}$ mice were collected, formalin-fixed, and paraffin-embedded. Subsequently, 4 μm-thick sections were stained with H&E, and lesion size and necrotic core area were determined in five sections per animal. Representative sections on separate slides were stained immunohistochemically with a macrophage-specific antibody (MAC-3; Becton & Dickinson) or a smooth muscle cell-specific antibody (α-smooth muscle cell actin; Sigma-Aldrich). Apoptosis was visualized using a terminal deoxytransferase dUTP nick-end labeling (TUNEL) kit (Roche; Woerden, Netherlands). Apoptotic cell content was determined by assessment of the TUNEL-positive area per section. Collagen was visualized by Sirius-Red staining of representative slides.

Cholesterol levels

Blood samples from *Apoe*$^{-/-MaFIA}$ and *Apoe*$^{-/-}$ mice were collected in tubes containing 5 μL 0.5M EDTA and centrifugated

for 10 min at 2100 rpm. Subsequently, plasma was isolated and used for total cholesterol measurement using a colorimetric assay (CHOD-PAP, Roche).

Flow cytometry

Upon sacrifice of the mice, blood, spleen, and bone marrow were collected. Single-cell suspensions were made from the spleen by crushing the tissue over a 70 μm cell strainer (BD Biosciences). Prior to measuring mature leukocytes in the spleen and bone marrow, erythrocytes were removed by incubation with hypotonic lysis buffer (8.4 g NH_4Cl and 0.84 g $NaHCO_3$ per liter distilled water). Samples and buffers were kept on ice throughout the experiment unless indicated otherwise. All measurements were performed on a FACS Canto II (BD Biosciences) and analysis of acquired data was performed using FACS Diva software (BD Biosciences).

To determine myeloid cell populations, blood and spleen samples were stained with CD45, CD11b, Ly6G, Ly6C, and CD115 (all from BD Biosciences). Nonspecific Fc-receptor binding was blocked by the addition of anti-CD16/CD32 antibody (eBioscience).

Myeloid progenitors were measured in the spleen and bone marrow. First, cells from the spleen and bone marrow were stained with biotin-conjugated antibodies against lineage markers (CD5, CD45RA [B220], CD11b, Gr-1 [Ly6C/G], 7-4, and Ter-119; Miltenyi Biotech). Next, lineage-positive cells were depleted using streptavidin-conjugated magnetic beads (Miltenyi Biotech) and LS columns (Miltenyi Biotech). Lineage-negative fractions were subsequently stained with antibodies for Sca-1, c-Kit (CD117), CD34, CD16/32, CD115, and lineage markers (CD5, CD45RA [B220], CD11b, Ly6C, Ly6G, Ter-119) (BD Biosciences) to verify effective enrichment (BD Biosciences).

Statistics

Data are expressed as mean ± SEM. All statistical analyses were performed using GraphPad Prism 9 (GraphPad Software Inc). Tests used to determine statistically significant differences are stated in the accompanying figure legends.

Results

Csf1r$^+$-specific apoptosis effectively depletes myeloid cells in vitro and in vivo

We first validated CSF1R (colony-stimulating factor 1 receptor or CD115) expression in human atherosclerosis at different stages of the disease. Stable atherosclerotic plaque segments have a thick fibrous cap that shields the plaque, making it less prone to rupture. Unstable plaque segments are covered by a thin fibrous cap and bear a larger lipid-rich necrotic core, increasing the risk for plaque rupture and a subsequent cardiovascular event [22].

Compared with stable plaque segments, *CSF1R* expression was increased in unstable plaques in a cohort of human carotid endarterectomy specimens (Fig. 1A). In addition, its expression was associated with unstable plaque characteristics (Fig. 1B) In Plaqview, a web application to explore various single-cell RNA sequencing data of atherosclerotic plaque tissue, we found that *CSF1R* expression in both human and murine atherosclerosis is restricted to myeloid cells (in particular to monocytes and macrophages) (Supporting Information Fig. S1 and S2) [23–26]. Thus, *Csf1r*-expressing cells are hereafter referred to as myeloid cells. To study the contribution of *Csf1r*-expressing myeloid cells in atherosclerotic plaque progression, we crossed MaFIA mice, carrying a suicide gene (encoding a fusion protein of Fas (aka TNFRSF6) and a mutant human FK506 binding protein-1A) under the control of the *Csf1r* promotor, with atherosclerosis-susceptible *Apoe*$^{-/-}$ mice. This fusion protein dimerizes upon binding to a drug, AP20187, leading to a *Csf1r*-specific apoptosis, and thereby Csf1R$^+$ mononuclear phagocyte cell depletion [11].

Atherogenesis was accelerated by perivascular collar placement [16]. Here, we have tested the effects of both systemic and local induction of myeloid-specific apoptosis. At the baseline level, no differences in blood monocytes (Supporting Information Fig. S3A) or in monocyte subsets (Supporting Information Fig. S3B–D) were detected. Leukocytes were also unaffected upon AP20187 administration apart from a small decrease in B lymphocyte numbers (Supporting Information Fig. S4). Because a previous study reported mild thrombocytopenia upon AP20187 administration [21], control *Apoe*$^{-/-}$ mice and the *Apoe*$^{-/-MaFIA}$ mice were given AP20187.

The effectiveness of AP20187 treatment on ablation of macrophages was verified in vitro using peritoneal macrophages isolated from *Apoe*$^{-/-}$ and *Apoe*$^{-/-MaFIA}$ mice. *Apoe*$^{-/-}$ control macrophages were unaffected by AP20187 treatment, while in the *Apoe*$^{-/-MaFIA}$ peritoneal macrophages, an almost complete induction of AP20187-dependent cell death (>80%) was observed (Fig. 2A).

After plaques were established, mice were injected with AP20187 to induce the depletion of myeloid cells and to assess their effect on atherogenesis. Pilot experiments pointed to a profound reduction of blood CSF1R$^+$ CD11b$^+$ myeloid cell numbers in *Apoe*$^{-/-MaFIA}$ mice after systemic treatment for 2 weeks using a dose of 1 mg/kg (Fig. 2B), demonstrating the effectiveness of the MaFIA approach in an in vivo atherosclerosis setting.

Systemic treatment with AP20187 induces depletion of plaque macrophages but does not affect atherosclerotic plaque burden

Next, we studied the effect of ablating plaque macrophages on atherosclerosis development. Hereto, *Apoe*$^{-/-MaFIA}$ and *Apoe*$^{-/-}$ mice were treated with 1 mg/kg AP20187 via IV injections in the tail vein every 3rd day, for 2 weeks, during which WTD feeding

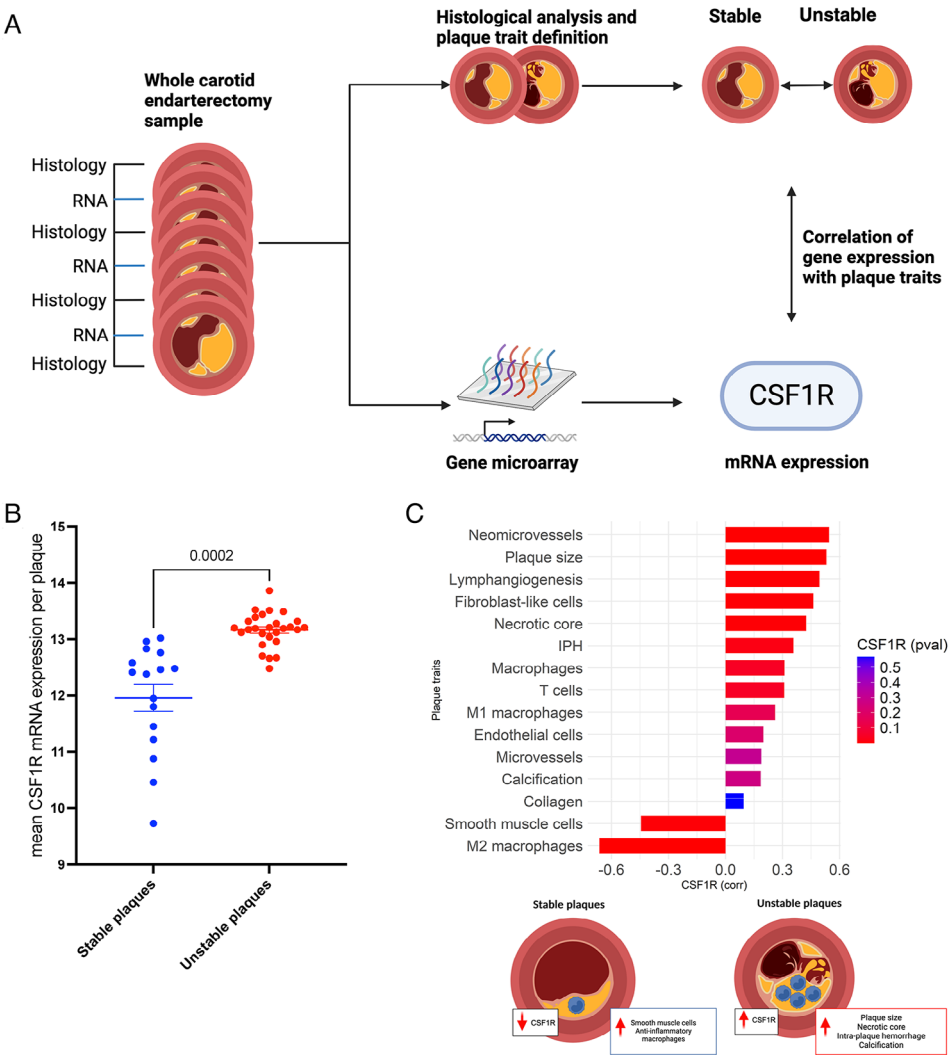

Figure 1. *CSF1R* expression is associated with features of advanced human atherosclerosis. (A) Experimental setup used to correlate gene expression analysis with histological features of human atherosclerotic plaques. (B) Association of *CSF1R* expression with stable vs. unstable plaque segments (n = 16 stable, n = 26 unstable, Welch's t-test, data are presented as ± SEM. p = 0.0002). (C) Correlation of *CSF1R* gene expression with histological atherosclerotic plaque characteristics.

was continued, after which mice were euthanized and plaques examined. Treatment with AP20187 did not influence plasma cholesterol levels (Supporting Information Fig. S5). After 2 weeks of treatment, *Apoe*$^{-/-MaFIA}$ mice did not display any changes in total plaque area (Fig. 3A) nor necrotic core size (Fig. 3B). As expected, an ablation of plaque macrophages was observed in the AP20187-treated *Apoe*$^{-/-MaFIA}$ mice compared with *Apoe*$^{-/-}$ controls (Fig. 3C). However, as ablation associated macrophage apoptosis had not affected the necrotic core size, this reduction could rather result from decreased monocyte migration toward the atherosclerotic lesion. In addition, a significant reduction in smooth muscle cells (SMC) in lesions from *Apoe*$^{-/-MaFIA}$ mice compared with control *Apoe*$^{-/-}$ mice was noted (Fig. 3D). To verify whether this was related to increased apoptosis of SMC, a TUNEL staining was performed. An almost fourfold increase in SMC apoptosis could be observed, indicating that also smooth muscle cells are directly or indirectly affected by the systemic treatment with AP20187 in vivo (Fig. 3E). Treatment did not affect smooth muscle cell apoptosis in the control mice and SMC in the plaque are not expressing *Csf1r* (Supporting Information Fig. S2). Thus, the observed increase in SMC apoptosis is likely to be directly or indirectly due to AP20187-induced myeloid cell ablation. Plaque collagen content was decreased in *Apoe*$^{-/-MaFIA}$ mice compared with *Apoe*$^{-/-}$ controls (p = 0.04; Fig. 3F). This decrease, together with the increased SMC apoptosis, was most likely responsible for the thinner fibrous caps observed in the *Apoe*$^{-/-MaFIA}$ lesions (Fig. 3G).

Myeloid cells are depleted systemically but recover after sustained AP20187 treatment

Because of the low impact of systemic AP20187 administration on atherosclerotic plaque phenotype, we quantified myeloid populations in the blood of AP20187-treated *Apoe*$^{-/-MaFIA}$ mice. Prolonged systemic treatment (1 mg/kg) resulted in an effective depletion of circulating (CD11b^{+}/Ly6G^{-}) monocytes, in *Apoe*$^{-/-MaFIA}$ mice in the first week of AP20187 treatment (Fig. 4A and B). Surprisingly, in view of the lack of CSF1R surface expression, also granulocyte numbers (CD11b^{+}/Ly6G^{+}) seemed to be affected, with a trend toward reduction after 1 week of treatment (Fig. 4A and C). Even more surprising was that monocyte and

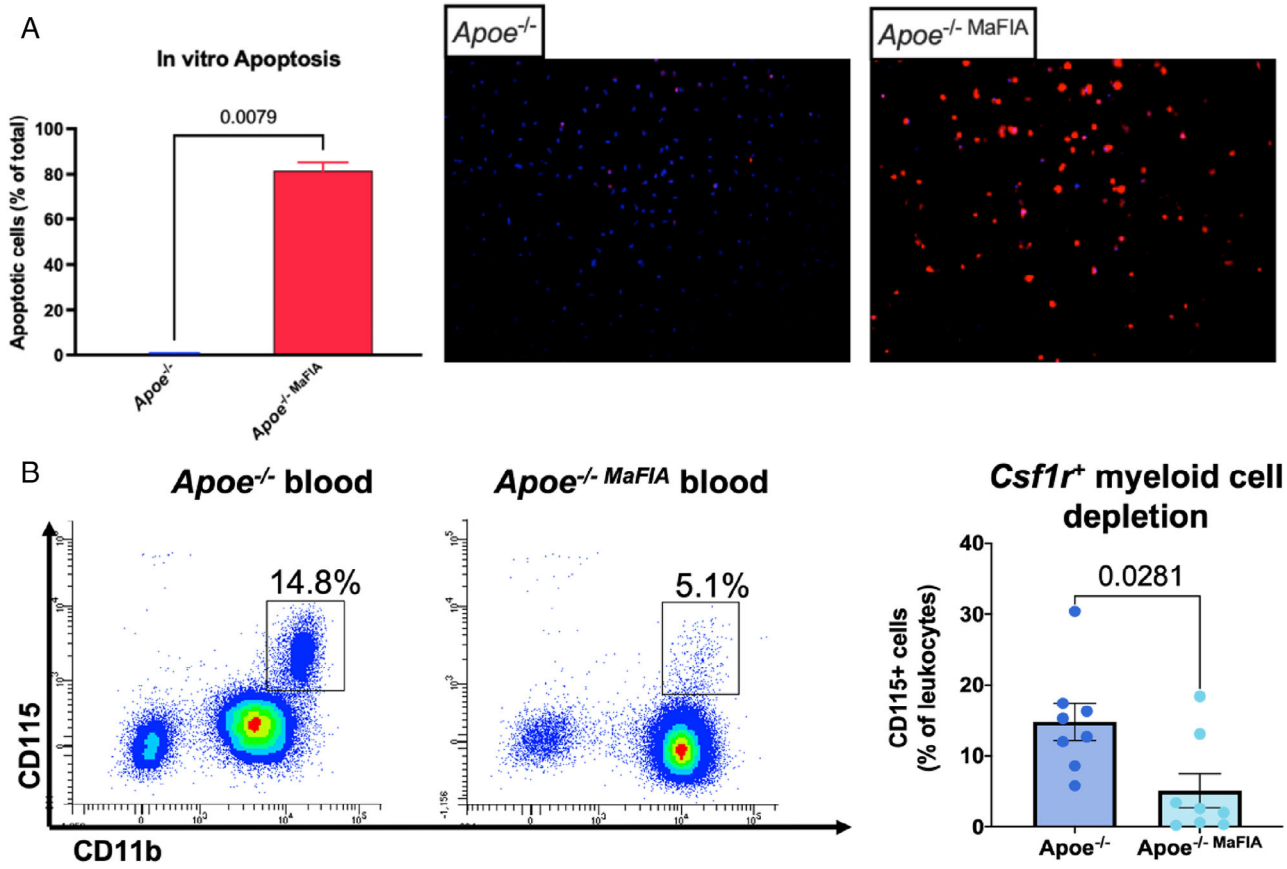

Figure 2. *Csf1r*$^{+}$-specific apoptosis induced myeloid cell apoptosis in vitro and in vivo. (A) In vitro induction of apoptosis in peritoneal macrophages from *Apoe*$^{-/-}$ and *Apoe*$^{-/-MaFIA}$ animals (n = 5 mice per group). Blue is DAPI (nuclei) and red is cleaved caspase 3 (apoptosis). Data are presented as mean ± SEM. p = 0.0079 (Mann–Whitney U test). (B) Depletion of *Csf1r*$^{+}$ cells (gated as life CD45^{+}/CD115^{+}/CD11b^{+}) in the blood of *Apoe*$^{-/-}$ and *Apoe*$^{-/-MaFIA}$ mice treated for 2 weeks with AP20187 (n = 8 per group). Data are presented as mean ± SEM. p = 0.0281 (Mann–Whitney U test).

granulocyte levels recovered to baseline values despite continuous AP20187 treatment in the second week of treatment (Fig. 4A–C). We also noted the appearance of an aberrant CD11b^{+}/Ly6G^{mid} myeloid subset, distinct from (mature) monocytes or granulocytes, after 1 and 2 weeks of treatment with AP20187 (Fig. 4A). Ly6C^{hi} monocytes were effectively depleted but recovered faster than the Ly6C^{int} or Ly6C^{lo} monocytes (Fig. 4D–G). This could be indicative of expanded production or release of Ly6C^{hi} monocytes from bone marrow and/or spleen in the AP20187-treated *Apoe*$^{-/-MaFIA}$ mice.

Myelopoiesis shifts to spleen after systemic AP20187 treatment

The rapid (albeit aberrant) recovery of circulating monocyte subsets after ablation points toward an induction of myelopoiesis. We therefore investigated myeloid cell populations in the spleen and bone marrow, known sites of myelopoiesis. Macroscopically, it could be noted that there was a clear distinction between the bones (femurs and tibiae) from *Apoe*$^{-/-}$ mice and *Apoe*$^{-/-MaFIA}$ mice treated with AP20187. *Apoe*$^{-/-MaFIA}$ mice had paler bone marrow which already indicated effects on bone marrow composition (Fig. 5A), which was confirmed by the decreased number of cells isolated from the bone marrow (Fig. 5B). Thus, we analyzed hematopoietic progenitor cells in more depth using lineage markers in combination with Sca-1, c-kit, and CD34 (Fig. 5C). Lineage^{-}/Sca-1^{-}/c-Kit^{+} (LK) cells were significantly diminished in bone marrow after 1 week of treatment (Fig. 5D). Within this LK fraction, the relative percentage of granulocyte/macrophage progenitors was increased, suggesting unchanged to slightly higher absolute counts of this progenitor subset in the bone marrow (Fig. 5E).

The analysis of splenic leukocytes revealed a significant increase in monocytes (Fig. 5G) and to a lower extent in granulocytes (not significant) (Fig. 5F) after 1 and 2 weeks of AP20187 treatment in *Apoe*$^{-/-MaFIA}$ mice. Flow cytometry revealed that CSF1R^{+} monocytes were almost completely ablated after AP20187 treatment (Fig. 5H), and remnant monocytes were CSF1R negative, similar to circulating monocytes in blood after treatment (Fig. 5B). In support of augmented splenic myelopoiesis after ablation, we observed strongly increased total cell counts in treated *Apoe*$^{-/-MaFIA}$ spleens (Fig. 5I). The splenic LSK fraction containing hematopoietic stem and progenitor cells was signifi-

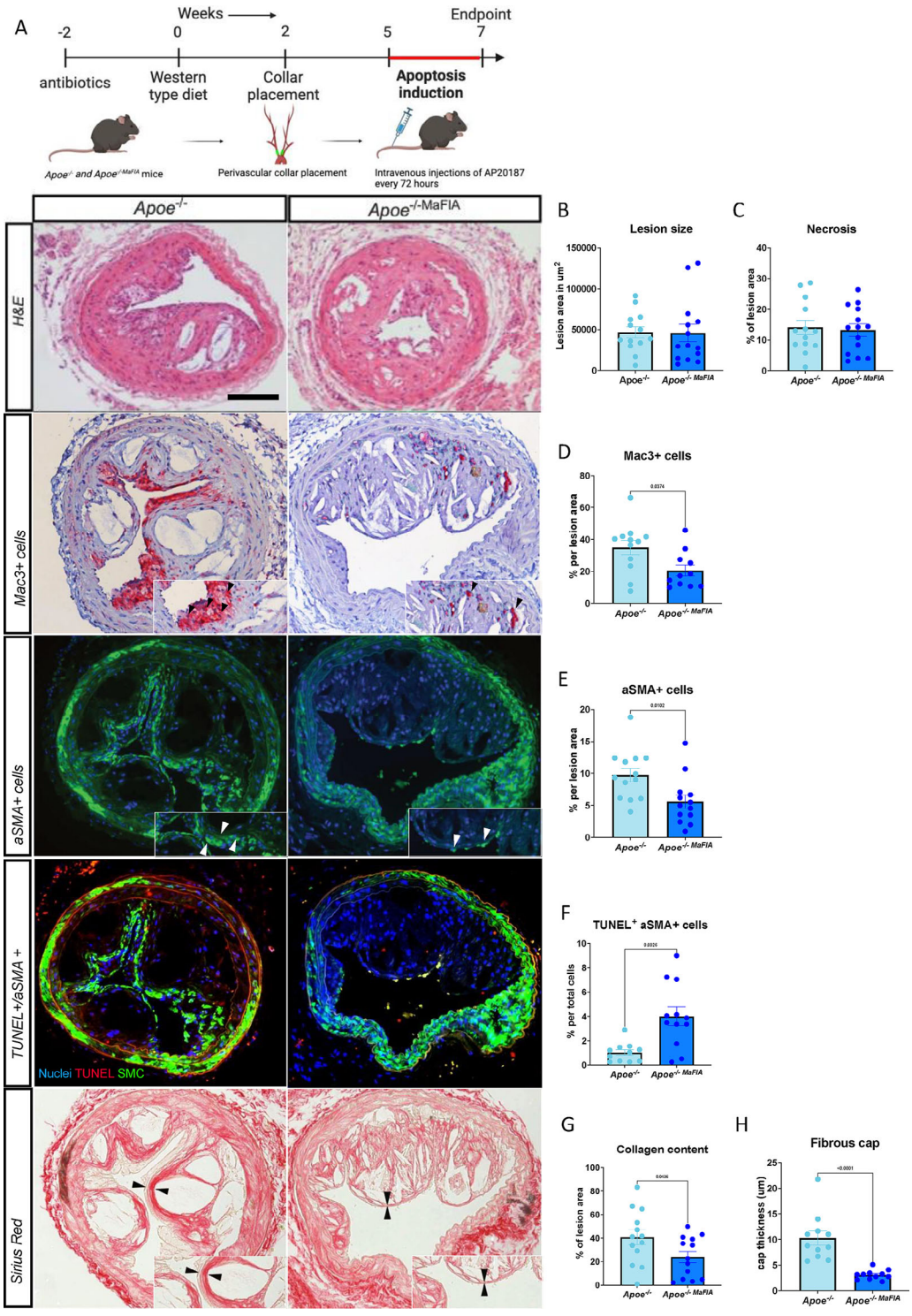

Figure 3. Systemic treatment with AP20187 reduced plaque macrophage and smooth muscle cell (SMC) content together with decreased collagen content without affecting lesion size and necrosis. (A) Experimental set-up for systemic *Csf1r*-specific apoptosis induction. *Apoe*$^{-/-}$ and *Apoe*$^{-/-MaFIA}$ animals on a Western-type diet received a perivascular collar for atherosclerosis induction. Three weeks after collar placement, mice received injections of 1 mg/kg of AP20187, by tail vein injections every 3rd day for 2 weeks before euthanasia. (B, C) Effects of systemic in vivo treatment on plaque area (B) and necrotic core area (C) were quantified on hematoxylin/eosin-stained aortic root sections. (D–H) Intimal macrophages content (D) and smooth muscle cells (E) in *Apoe*$^{-/-MaFIA}$ animals upon AP20187 treatment, measured by macrophage (Mac3) and alpha-smooth muscle cell actin (αSMA) staining in aortic root sections, respectively. Further, SMC apoptosis was quantified by TUNEL-staining (F). Collagen content (G) and cap thickness (H) were determined from Sirius-Red stained sections. Representative pictures of each staining are shown (n = 10–13 *Apoe*$^{-/-}$ and n = 7–14 *Apoe*$^{-/-MaFIA}$ animals). Data are presented as mean ± SEM, with each dot representing one individual mouse. P-values <0.05 (unpaired T-tests) are indicated. The scale bar represents 100 μm.

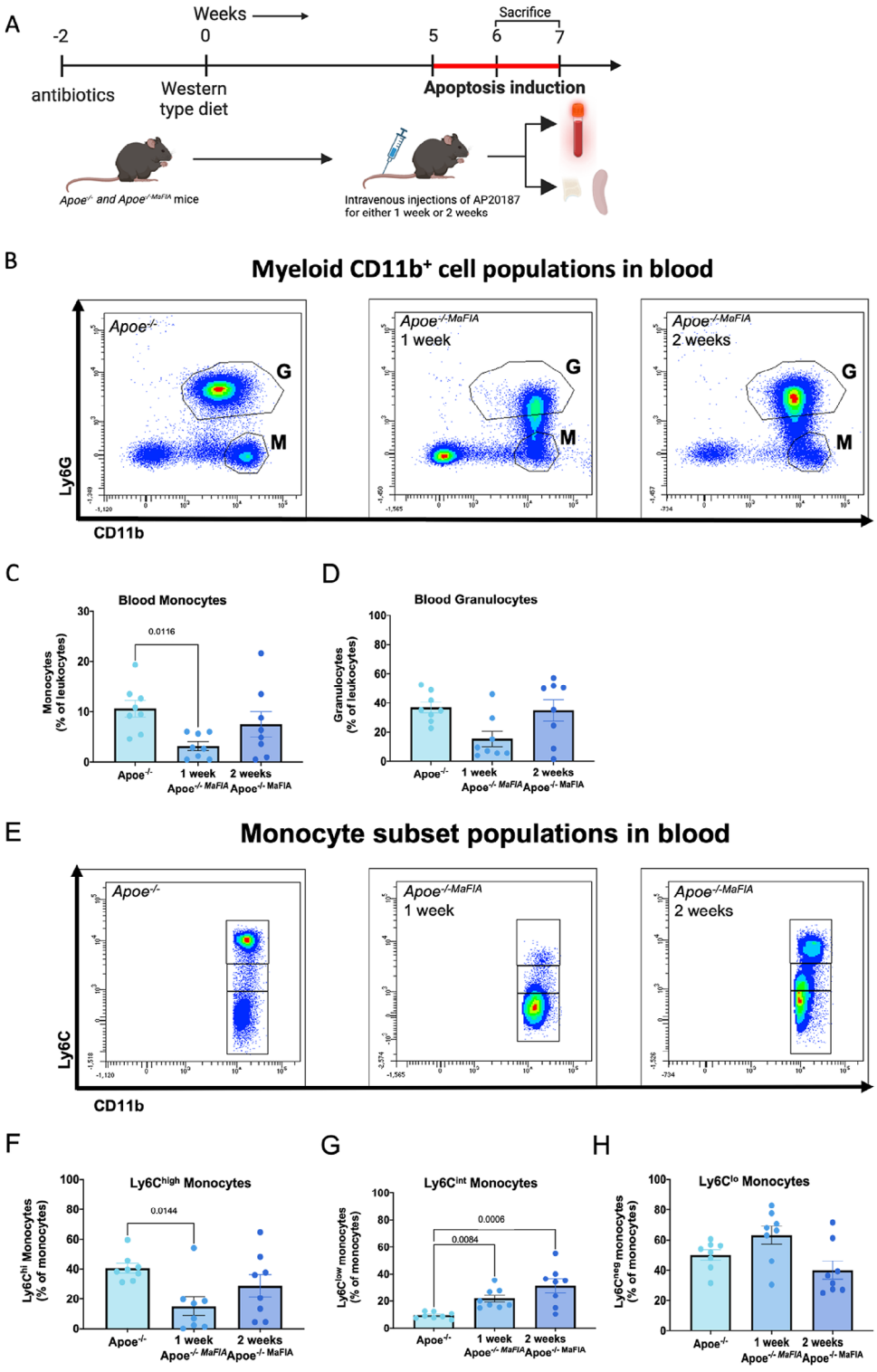

Figure 4. Sustained treatment with AP20187 resulted in disturbed circulating leukocyte patterns and a shift in blood monocyte subsets. (A) Experimental design of the systemic ablation experiment. Mice were put on a Western-type diet at week 2 and *Csf1r*-specific apoptosis was induced at week 5 for either 1 week or 2 weeks before sacrifice. Mice received injections of 1 mg/kg of AP20187 by tail vein injections every 3rd day. (B) Circulating myeloid cell patterns in the blood of *Apoe*$^{-/-}$ (left panel, negative control) and *Apoe*$^{-/-MaFIA}$ mice at 1 week (mid panel) and at 2 weeks (right panel) of AP20187 treatment. Representative dot plots of monocytes (M, gated as live CD45^{+} Ly6G^{-} CD11b^{high}) and granulocytes (G, gated as live CD45^{+} Ly6G^{+} CD11b^{+}) are shown (C) Effects on monocytes and granulocytes (D) after 1 and 2 weeks of treatment with AP20187. (E) Representative dot plots of monocyte subsets, Ly6C and CD11b. Relative levels of s Ly6C^{hi} (F), Ly6C^{int} (G), and Ly6C^{lo} (H) monocyte subsets over the course of the AP20187 treatment are shown. N = 8 animals per group; data are presented as mean ± SEM. Only *p*-values < 0.05 are indicated (Kruskal–Wallis test with pairwise comparisons).

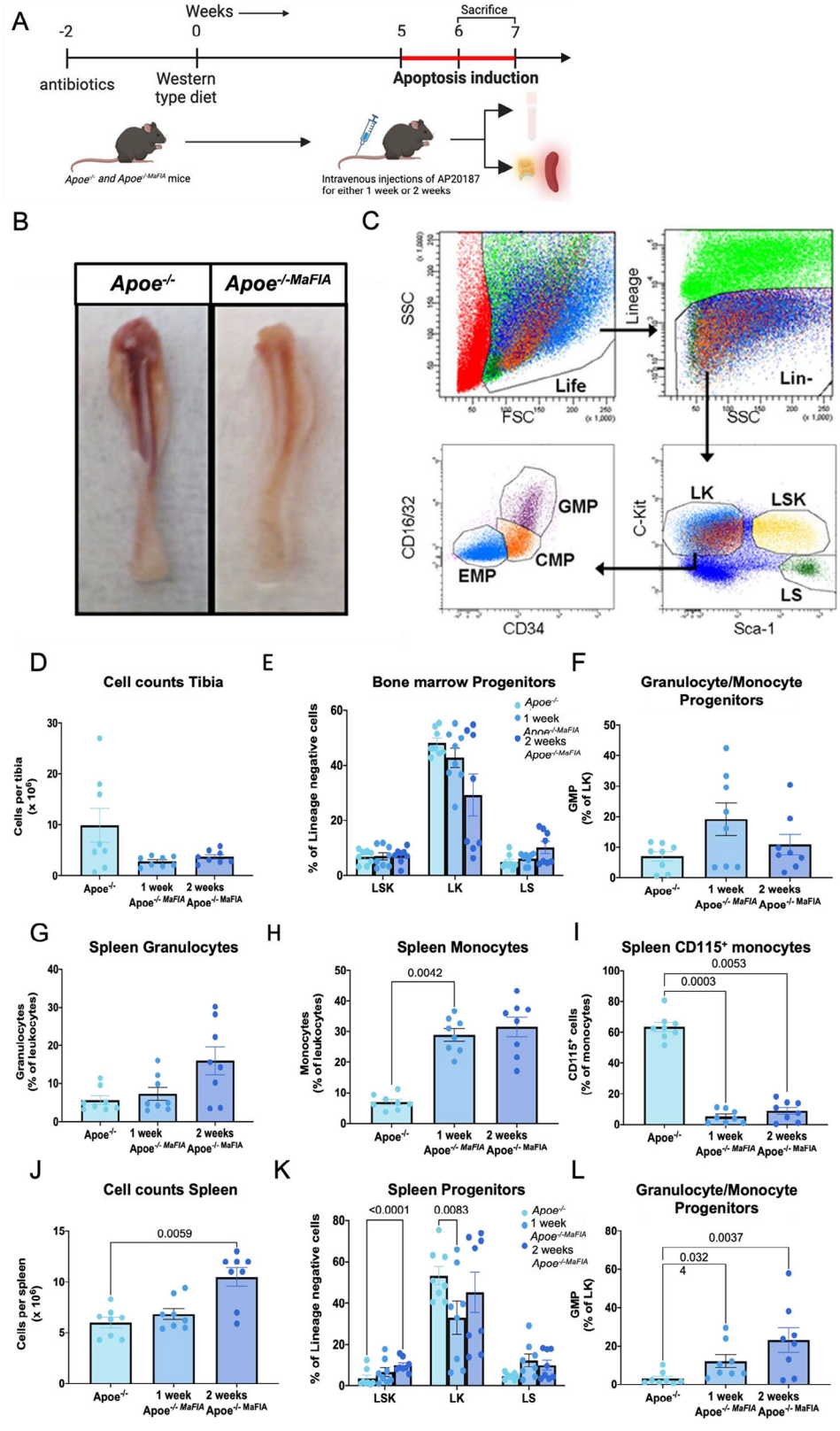

Figure 5. Systemic treatment with AP20187 induced extramedullary myelopoiesis. (A) Effects of the sustained systemic *Csf1r*-specific apoptosis induction on bone marrow and splenic monopoiesis, measured after 1 and 2 week(s) of AP20187 treatment (IV injection, every 3rd day for 2 weeks). (B) Macroscopic images of femurs from AP20187 treated $Apoe^{-/-}$ and $Apoe^{-/-MaFIA}$ mice. (C) Representative dot plots indicating relevant gating strategy to identify hematopoietic stem cell populations in the bone marrow. (D) Total cells in the tibia bone marrow after 1 and 2 weeks of AP20187 treatment. Differences in bone marrow progenitor populations are shown after 1 and 2 weeks of AP20187 treatment (E) and the granulocyte/macrophage progenitors (GMP within the LK (Lineage$^-$/Sca-1$^-$/c-Kit$^+$) (F). Granulocytes (G) and monocytes (H) in the spleen are shown after treatment of $Apoe^{-/-MaFIA}$ mice with 1 mg/kg AP20187. Total spleen cellularity AP20187 treatment in $Apoe^{-/-MaFIA}$ mice was measured (I) and changes in spleen progenitors are displayed (K) Within the Lineage$^-$/Sca-1$^-$/c-Kit$^+$ (LK) changes in granulocyte/macrophage progenitors (GMP) are shown (K). $N = 8$ animals per group; data are presented as mean ± SEM; p-values < 0.05 (Kruskal–Wallis test with pairwise comparisons) are indicated.

cantly increased after 2 weeks of AP20187 treatment, while the LK fraction containing the myeloid progenitor cells was reduced after 1 week but recovered at 2 weeks of treatment (Fig. 5J). Remarkably, the initial decrease in LK cells was accompanied by an increase in granulocyte-monocyte progenitor cells after both one and 2 weeks of treatment, suggesting an increasingly active monocytopoiesis in the spleen (Fig. 5K). Notably, we also observed a reduction in the EMP fraction upon systemic treatment of *Apoe*$^{-/-MaFIA}$ mice with AP20187 (Supporting Information Fig. S6).

Local treatment with AP20187 decreases plaque burden together with reduced macrophage content

The observed effects of systemic AP20187 administration on myeloid cell expansion led us to design a second atherosclerosis study in which animals received a collar around the carotid arteries combined with an osmotic minipump with catheters attached to the perivascular side of the carotid arteries near the collar for a site-restricted induction of myeloid-cell apoptosis. AP20187 was continuously delivered for 2 weeks at a cumulative dose of 0.01 mg/kg body weight. Analysis of the carotid arteries after 2 weeks of treatment showed that total plaque area ($p = 0.047$; Fig. 6A) but not necrotic core formation (Fig. 6B) was decreased when the *Apoe*$^{-/-\mathrm{MaFIA}}$ animals were treated locally, compared with treated *Apoe*$^{-/-}$ controls. As expected, macrophages were decreased in the plaques of *Apoe*$^{-/-\mathrm{MaFIA}}$ mice compared with the controls, in line with the decreased plaque area (Fig. 6C). In contrast to systemic delivery, intraplaque smooth muscle cell content and apoptosis were not affected by the local treatment with AP20187(Fig. 6D and E) and neither were collagen content and fibrous cap thickness (Fig. 6F and G). When mice received the local AP20187 treatment, circulating monocytes were increased without any further impact on monocyte subsets between *Apoe*$^{-/-MaFIA}$ mice and *Apoe*$^{-/-}$ controls (Supporting Information Fig. S7).

Discussion

Macrophages are essential in atherosclerotic lesion development at all stages and potentially contribute to clinical outcomes by destabilizing the atherosclerotic lesion [27, 28]. Although their involvement in atherosclerosis was corroborated by experimental interventions in macrophage influx and macrophage CSF1 signaling [6, 8, 10], studies on conditional depletion of CD11b^{+} macrophages [29] in atherosclerosis were less conclusive. Deploying a Fas-dependent conditional myeloid cell depletion model, the MaFIA [11], on an Apoe$^{-/-}$ background, we show that systemic depletion of macrophages did not affect plaque burden, despite reductions in plaque resident macrophage and SMC content. Interestingly, a profound *Csf1r*-independent splenic myelopoiesis was detected after 1 week of depletion together with the emergence of an aberrant granulocyte population and a marked Ly6Chigh-to-low monocyte subset shift. This may have masked potential effects of macrophage ablation on the atherosclerotic plaque phenotype. Indeed, prolonged local administration of AP20187 did not only reduce intimal macrophage content but also plaque size, suggesting the detrimental role of *Csf1r* expressing plaque macrophages at later stages of atherosclerosis in mice.

For these studies, we used the MaFIA model, where administration of AP20187 induces dimerization of an engineered FKBP/Fas fusion protein that triggers the extrinsic pathway of cell apoptosis [11]. Unlike the DTR model, which relies on the administration of diphtheria toxin, and which has been reported to be less suited for mid- to long-term administration [30–32], treatment with AP20187 is generally tolerated well and has higher tissue penetrating capacity.

Systemic ablation led to a reduction in plaque macrophage content but also vascular smooth muscle cells (vSMC). Although we cannot exclude that this is indirectly due to the increased macrophage cell death, this could well reflect *Csfr1* expression by transdifferentiated plaque vSMC, as has been shown before [26, 33, 34]. These vSMC show also other characteristics of the monocyte/macrophage lineage such as phagocytic capacity and even can develop into foam cells among other macrophage subsets [26, 33, 35]. Interestingly, *Csf1r* expression was seen in a macrophage subset that was shown to be SMC lineage positive (Mac2; Supporting Information Fig. S2) [26]. However, *Csf1r* expression was not observed directly in SMC-cell subsets in the murine atherosclerotic plaque and more importantly, SMC-apoptosis was not affected in the local set-up (Supporting Information Fig. S2; Fig. 6). Thus, SMC-apoptosis is most likely indirectly affected by systemic AP20187 administration.

Regardless of these changes, the increased apoptosis of vSMC and macrophages did not result in any changes in atherosclerotic plaque burden after a 2-week *Csf1r*-specific apoptosis induction.

As expected, AP20187 injection led to a profound decrease in total leukocyte numbers in blood and spleen in the first week of treatment, with ablation of monocyte subsets and granulocytes and only minor effects on B lymphocytes (Fig S4). The effects on granulocytes and B-cells were, in part, unexpected, however, this could be explained by the role of PU.1 in controlling M-CSF receptor expression [36, 37]. PU.1 has already been shown to be involved in both myeloid and B cell development in a PU.1 knock-out model [38] and may transiently activate transcription of the M-CSF receptor, and thus also of the MaFIA transgene. Indeed, granulocytes were seen to be GFP^{+} although they did not express surface CSF1R. In the murine plaque, *Csf1r* expression in neutrophils can be observed to a low extent in single-cell RNA sequencing data (Supporting Information Fig S2). A transient expression of *Csf1r* by granulocytes could have implications for our knowledge of myelopoiesis and cell maturation. Further, prolonged systemic depletion of *Csf1r*$^{+}$ myeloid cells was followed by disturbed myelopoiesis with increased extramedullar myelopoiesis, shifts toward nonclassical (Ly6c^{lo}) and intermediate monocyte subsets (Ly6C^{int}), and release of immature myelocytes into the circulation. This rebound of the monocyte lineage has previously been described, but we are the first to link this

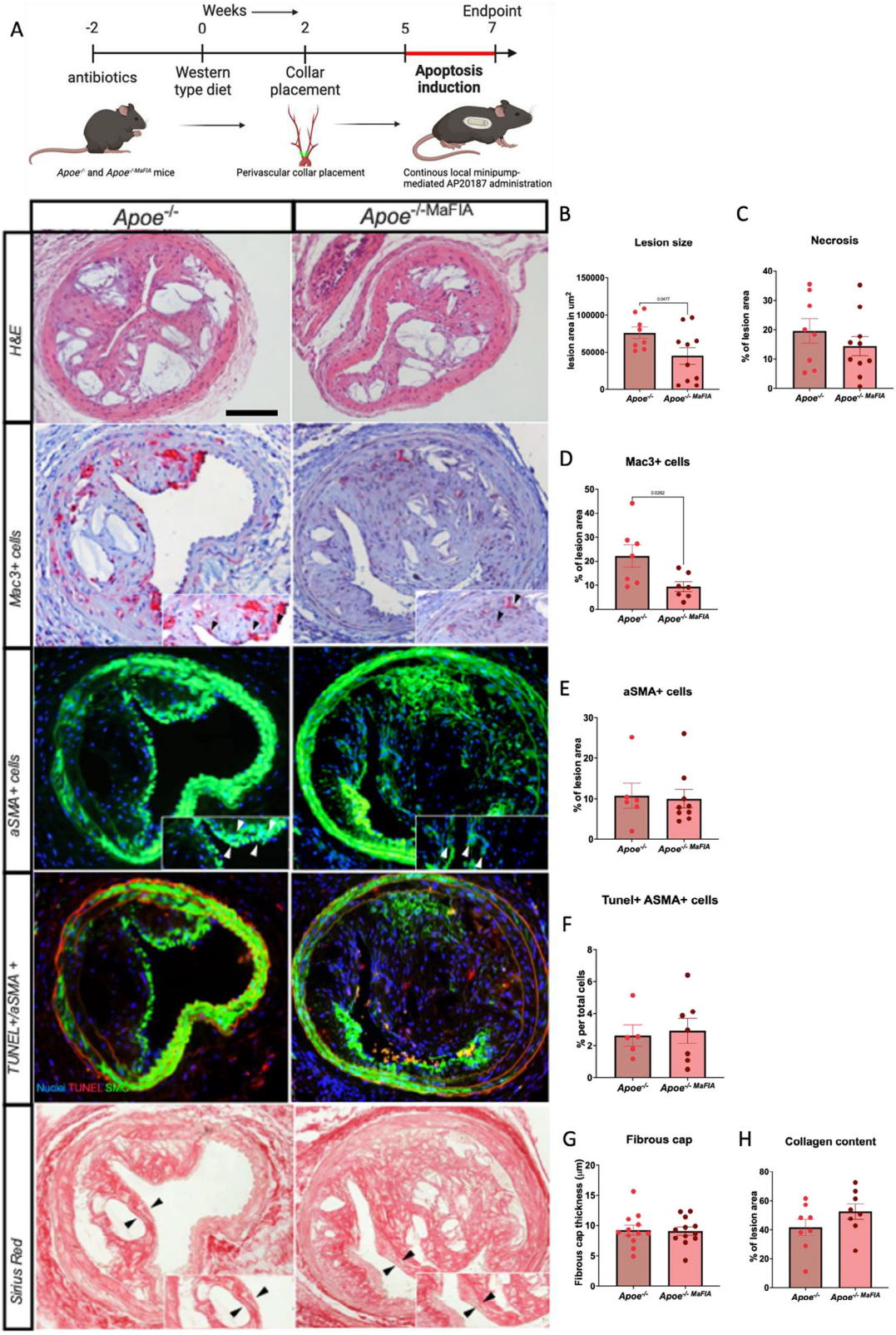

Figure 6. Local treatment with AP20187 reduced plaque size and macrophage content without affecting SMC presence. (A) Experimental set-up for local *Csf1r*-specific apoptosis induction. *Apoe*$^{-/-}$ and *Apoe*$^{-/-MaFIA}$ animals on a Western-type diet received a perivascular collar for atherosclerosis induction. After 3 weeks, mice received an osmotic minipump implanted at the perivascular site of the carotid artery and subjected to continuous AP20187 administration at a dose of 0.01 mg/kg of AP20187 for 2 weeks before sacrifice. (B, C) Effects of osmotic minipump-aided delivery of AP20187 (0.01 mg/kg continuously, for 2 weeks) on plaque (B) and necrotic core area (C). Plaque size was quantified on hematoxylin/eosin-stained aortic

root sections. (D–H) Intimal macrophage (D) and smooth muscle cell content (E) in AP20187 treated *Apoe*$^{-/-MaFIA}$ mice, measured by macrophage (Mac3) and alpha-smooth muscle cell actin (αSMA) staining of aortic root sections, respectively. (F) Effects on plaque SMC apoptosis were quantified by TUNEL-staining (F). Plaque collagen content (G) and cap thickness (H) were visualized by Sirius-Red staining. Representative pictures of each staining are shown (n = 5–8 *Apoe*$^{-/-}$ and n = 7–10 *Apoe*$^{-/-MaFIA}$ animals). Data are presented as mean ± SEM, with each dot representing an individual mouse. P-values < 0.05 (unpaired T-tests) are indicated. The scale bar represents 100 μm.

replenishment to increased extramedullary hematopoiesis and to provide proof that this is accompanied by a shift in circulating monocyte subset distribution toward a nonclassical phenotype [11]. The production and release of myeloid progenitors in the bone marrow are controlled by osteoclasts [39], which express several macrophage surface markers, including CSF1R [4], and which were depleted as well after in vivo AP20187 treatment [4, 40]. The failing stromal myelopoiesis could have spurred extramedullary myelopoiesis in the spleen observed after prolonged depletion. The bulk of the emerging myeloid subsets is deficient to low in CSF1R, which suggests that another myeloid mitogen, such as GM-CSF, might take over to drive the myelopoiesis. Moreover, we observed a clear shift from Ly6C^{hi} to Ly6C$^{int/lo}$ monocytes, with direct repercussions on the function of monocytes and subsequent macrophages [41–43]. This shift could be driven either by a decreased survival of Ly6C^{hi}CSF1R^{+} monocytes or an accelerated transition from classical to nonclassical monocytes. Collectively, the net effect of the compensatory myelopoiesis is difficult to estimate. On the one hand, the intermediate monocyte expansion is generally considered detrimental, while the shift toward the nonclassical monocytes may improve patrolling capacity and innate immune defense functions and is thus considered protective [44]. Finally, GM-CSF (CSF-2) dominated monocyte/macrophage maturation may be perceived as proatherogenic [45]. Additional study is needed to integrate these effects. Further, we observed a reduction in the EMP fraction upon systemic treatment of *Apoe*$^{-/-MaFIA}$ mice with AP20187 (Fig S6) possibly explaining the visibly paler bone marrow (Fig 5B).

The myeloid expansion after systemic AP20187 treatment also prompted the study of the plaque-specific effects of macrophage ablation, administering the compound by an osmotic minipump eluting at the plaque adventitia. This site-restricted administration of AP20187 only induced marginal systemic effects, confirming the local nature of the intervention (Supporting Information Fig. S7). Moreover, it resulted in a strong reduction of intimal macrophage numbers, confirming effective ablation. In contrast to systemic myeloid cell depletion, it led to a significant decrease in plaque size. As the impact on circulating myeloid cells was marginal, the beneficial effect on plaque burden and the decrease in macrophage content indicates that *Csf1r*$^{+}$ cell apoptosis is only efficiently inhibiting atherogenesis when locally restricted, suggesting that the circulating monocyte pool may compensate for the local loss of plaque resident macrophages.

Analysis of murine single-cell RNA sequencing data showed that *Csf1r* expression is enriched in foam-cell-like macrophages (Supporting Information Fig S2; Mac1 and Mac3 in Conklin et al. [*26*]). This might suggest that under diffusion-limited conditions AP20187 will preferentially induce apoptosis in plaque foam cells. Further studies are required to corroborate these findings and map the impact of AP20187-induced *Csf1R*$^{+}$ cell depletion on the plaque macrophage phenotypes.

We can conclude that macrophages and other CSF-1 receptor-positive cells are critical controllers of many processes including hematopoiesis and atherosclerosis development. While systemic macrophage depletion did not affect plaque burden, it led to a decrease in plaque macrophages and SMC content together with the induction of splenic myelopoiesis and a shift from circulating classical monocytes toward nonclassical monocyte subsets. In contrast, local macrophage depletion led to a decrease in plaque burden without major systemic effects on the circulating monocyte landscape.

Overall, the depletion of macrophages results in disturbed physiology indicative of the essential role of myeloid cells in maintaining health.

Data limitations and perspectives

This study has several limitations. While we have shown that the induction of systemic myeloid cell apoptosis leads to an increased extramedullary myelopoiesis together with elevated circulating nonclassical monocyte numbers, our study setup did not allow examining the contribution of these cells to atherosclerotic plaque formation. Similarly, although we observed a decrease in plaque macrophage content, we did not explore how the depletion differentially affects macrophage subsets. Further studies using state-of-the-art spatial phenotyping methods will be necessary to elucidate these aspects.

In summary, we successfully demonstrate the utility of the MaFIA myeloid cell depletion model in studying macrophage contributions to atherosclerosis. Notably, we are the first to link the previously described rebound of circulating monocytes after transient myeloid cell depletion to the induction of extramedullary myelopoiesis and the shift in monocyte subsets toward nonclassical monocytes. Furthermore, we highlight the value of using local depletion approaches when studying the impact of plaque resident macrophages on atherosclerosis.

Acknowledgements: This work was performed within the framework of the Center for Translational Molecular Medicine (CTMM; http://www.ctmm.nl), project CIRCULATING CELLS (grant number 01C-102) and was supported by the Dutch Heart Foundation (Dekker 2020T042 to P.G.). The dimerizing drug (AP20187) used

to induce ablation of *Csf1r* expressing cells in the in vitro and in vivo experiments was a kind gift from Ariad Pharmaceuticals.

Conflict of interest: The authors declare no conflict of interest.

Author contributions: Indira Medina, Jeroen J.T. Otten, and Elias B. Wieland performed the experimental studies. I. Medina, Elias B. Wieland, Lieve Temmerman, Jeroen J.T. Otten, Erik A.L. Biessen, and Pieter Goossens analyzed the data. Erik A.L. Biessen, Elias B. Wieland, and Lieve Temmerman wrote the manuscript. Pieter Goossens, Erik A.L. Biessen, and Theo J.C. Van Berkel made critical edits to the manuscript. Beatriz Bermudez, Ilze Bot, Timo Rademakers, Erwin Wijnands, Leon Schurgers, and Pieter Goossens provided essential expertise and help with the experiments. Barend Mees helped with the buildup of the Carotid endarterectomy (CEA) tissue biobank.

Data availability statement: The data that support the findings of this study are available from the corresponding author upon reasonable request. Single-cell RNA sequencing data of human [24, 25, 46] and murine atherosclerotic plaque [26] is publicly available and can be retrieved on Plaqview [23].

References

1 **Bjorkegren, J. L. M. and Lusis, A. J.**, Atherosclerosis: recent developments. *Cell* 2022. **185**: 1630–1645.

2 **Robbins, C. S., Hilgendorf, I., Weber, G. F., Theurl, I., Iwamoto, Y., Figueiredo, J. L., Gorbatov, R. et al.**, Local proliferation dominates lesional macrophage accumulation in atherosclerosis. *Nat. Med.* 2013. **19**: 1166–1172.

3 **Hardtner, C., Kornemann, J., Krebs, K., Ehlert, C. A., Jander, A., Zou, J., Starz, C. et al.**, Inhibition of macrophage proliferation dominates plaque regression in response to cholesterol lowering. *Basic Res. Cardiol.* 2020. **115**: 78.

4 **Cecchini, M. G., Hofstetter, W., Halasy, J., Wetterwald, A. and Felix, R.**, Role of CSF-1 in bone and bone marrow development. *Mol. Reprod. Dev.* 1997. **46**: 75–83.

5 **Di Gregoli, K. and Johnson, J. L.**, Role of colony-stimulating factors in atherosclerosis. *Curr. Opin. Lipidol.* 2012. **23**: 412–421.

6 **Sinha, S. K., Miikeda, A., Fouladian, Z., Mehrabian, M., Edillor, C., Shih, D., Zhou, Z. et al.**, Local M-CSF (macrophage colony-stimulating factor) expression regulates macrophage proliferation and apoptosis in atherosclerosis. *Arterioscler. Thromb. Vasc. Biol.* 2021. **41**: 220–233.

7 **Qiao, J. H., Tripathi, J., Mishra, N. K., Cai, Y., Tripathi, S., Wang, X. P., Imes, S. et al.**, Role of macrophage colony-stimulating factor in atherosclerosis: studies of osteopetrotic mice. *Am. J. Pathol.* 1997. **150**: 1687–1699.

8 **Rajavashisth, T., Qiao, J. H., Tripathi, S., Tripathi, J., Mishra, N., Hua, M., Wang, X. P. et al.**, Heterozygous osteopetrotic (op) mutation reduces atherosclerosis in LDL receptor- deficient mice. *J. Clin. Invest.* 1998. **101**: 2702–2710.

9 **Smith, J. D., Trogan, E., Ginsberg, M., Grigaux, C., Tian, J. and Miyata, M.**, Decreased atherosclerosis in mice deficient in both macrophage colony-stimulating factor (op) and apolipoprotein E. *Proc. Natl. Acad. Sci. U S A.* 1995. **92**: 8264–8268.

10 **Shaposhnik, Z., Wang, X. and Lusis, A. J.**, Arterial colony stimulating factor-1 influences atherosclerotic lesions by regulating monocyte migration and apoptosis. *J. Lipid Res.* 2010. **51**: 1962–1970.

11 **Burnett, S. H., Kershen, E. J., Zhang, J., Zeng, L., Straley, S. C., Kaplan, A. M. and Cohen, D. A.**, Conditional macrophage ablation in transgenic mice expressing a Fas-based suicide gene. *J. Leukoc. Biol.* 2004. **75**: 612–623.

12 **Wu, C. L., McNeill, J., Goon, K., Little, D., Kimmerling, K., Huebner, J., Kraus, V. et al.**, Conditional macrophage depletion increases inflammation and does not inhibit the development of osteoarthritis in obese macrophage Fas-induced apoptosis-transgenic mice. *Arthritis Rheumatol* 2017. **69**: 1772–1783.

13 **Gabrusiewicz, K., Hossain, M. B., Cortes-Santiago, N., Fan, X., Kaminska, B., Marini, F. C., Fueyo, J. et al.**, Macrophage Ablation Reduces M2-like populations and jeopardizes tumor growth in a MAFIA-based glioma model. *Neoplasia* 2015. **17**: 374–384.

14 **Clifford, A. B., Elnaggar, A. M., Robison, R. A. and O'Neill, K.**, Investigating the role of macrophages in tumor formation using a MaFIA mouse model. *Oncol. Rep.* 2013. **30**: 890–896.

15 **Plump, A. S., Smith, J. D., Hayek, T., Aalto-Setala, K., Walsh, A., Verstuyft, J. G., Rubin, E. M. et al.**, Severe hypercholesterolemia and atherosclerosis in apolipoprotein E-deficient mice created by homologous recombination in ES cells. *Cell* 1992. **71**: 343–353.

16 **von der Thusen, J. H., van Berkel, T. J. and Biessen, E. A.**, Induction of rapid atherogenesis by perivascular carotid collar placement in apolipoprotein E-deficient and low-density lipoprotein receptor-deficient mice. *Circulation* 2001. **103**: 1164–1170.

17 **Jin, H., Goossens, P., Juhasz, P., Eijgelaar, W., Manca, M., Karel, J. M. H., Smirnov, E. et al.**, Integrative multiomics analysis of human atherosclerosis reveals a serum response factor-driven network associated with intraplaque hemorrhage. *Clin. Transl. Med.* 2021. **11**: e458.

18 **Du, P., Kibbe, W. A. and Lin, S. M.**, lumi: a pipeline for processing Illumina microarray. *Bioinformatics* 2008. **24**: 1547–1548.

19 **Ritchie, M. E., Phipson, B., Wu, D., Hu, Y., Law, C. W., Shi, W. and Smyth, G. K.**, limma powers differential expression analyses for RNA-sequencing and microarray studies. *Nucleic. Acids. Res.* 2015. **43**: e47.

20 **Jin, H., Mees, B. M. E., Biessen, E. A. L. and Sluimer, J. C.**, Transcriptional sex dimorphism in human atherosclerosis relates to plaque type. *Circ. Res.* 2021. **129**: 1175–1177.

21 **Neff, T., Horn, P. A., Valli, V. E., Gown, A. M., Wardwell, S., Wood, B. L., von Kalle, C. et al.**, Pharmacologically regulated in vivo selection in a large animal. *Blood* 2002. **100**: 2026–2031.

22 **Virmani, R., Kolodgie, F. D., Burke, A. P., Farb, A. and Schwartz, S. M.**, Lessons from sudden coronary death: a comprehensive morphological classification scheme for atherosclerotic lesions. *Arterioscler. Thromb. Vasc. Biol.* 2000. **20**: 1262–1275.

23 **Ma, W. F., Hodonsky, C. J., Turner, A. W., Wong, D., Song, Y., Mosquera, J. V., Ligay, A. V. et al.**, Enhanced single-cell RNA-seq workflow reveals coronary artery disease cellular cross-talk and candidate drug targets. *Atherosclerosis* 2022. **340**: 12–22.

24 **Zernecke, A., Erhard, F., Weinberger, T., Schulz, C., Ley, K., Saliba, A. E. et al.**, Integrated single-cell analysis based classification of vascular mononuclear phagocytes in mouse and human atherosclerosis. *Cardiovasc. Res.* 2023. **119**: 1676–1689.

25 **Alsaigh, T., Evans, D., Frankel, D. and Torkamani, D.**, Decoding the transcriptome of atherosclerotic plaque at single-cell resolution. *Biorxiv* 2020.

26 **Conklin, A. C., Nishi, H., Schlamp, F., Ord, T., Ounap, K., Kaikkonen, M. U., Fisher, E. A. et al.**, Meta-analysis of smooth muscle lineage transcriptomes in atherosclerosis and their relationships to in vitro models. *Immunometabolism* 2021. **3**: e210022.

27 Periodical27. **Legein, B.**, **Temmerman, L.**, **Biessen, E. A. and Lutgens, E.**, Inflammation and immune system interactions in atherosclerosis. *Cell Mol. Life Sci.* 2013. **70**: 3847–3869.

28 **Ross, R.**, Atherosclerosis–an inflammatory disease. *N. Engl. J. Med.* 1999. **340**: 115–126.

29 **Stoneman, V.**, **Braganza, D.**, **Figg, N.**, **Mercer, J.**, **Lang, R.**, **Goddard, M. and Bennett, M.**, Monocyte/macrophage suppression in CD11b diphtheria toxin receptor transgenic mice differentially affects atherogenesis and established plaques. *Circ. Res.* 2007. **100**: 884–893.

30 **Goldwich, A.**, **Steinkasserer, A.**, **Gessner, A. and Amann, K.**, Impairment of podocyte function by diphtheria toxin–a new reversible proteinuria model in mice. *Lab. Invest.* 2012. **92**: 1674–1685.

31 **Rubino, S. J.**, **Mayo, L.**, **Wimmer, I.**, **Siedler, V.**, **Brunner, F.**, **Hametner, S. Madi, A. et al.**, Acute microglia ablation induces neurodegeneration in the somatosensory system. *Nat. Commun.* 2018. **9**: 4578.

32 **Peng, J.**, **Zou, Q.**, **Chen, M. J.**, **Ma, C. L. and Li, B. M.**, Motor deficits seen in microglial ablation mice could be due to non-specific damage from high dose diphtheria toxin treatment. *Nat. Commun.* 2022. **13**: 3874.

33 **Herembert, T.**, **Gogusev, J.**, **Zhu, D. L.**, **Drueke, T. B. and Marche, P.**, Control of vascular smooth-muscle cell growth by macrophage-colony-stimulating factor. *Biochem. J.* 1997. **325**: 123–128.

34 **Inaba, T.**, **Yamada, N.**, **Gotoda, T.**, **Shimano, H.**, **Shimada, M.**, **Momomura, K.**, **Kadowaki, T. et al.**, Expression of M-CSF receptor encoded by c-fms on smooth muscle cells derived from arteriosclerotic lesion. *J. Biol. Chem.* 1992. **267**: 5693–5699.

35 **Feil, S.**, **Fehrenbacher, B.**, **Lukowski, R.**, **Essmann, F.**, **Schulze-Osthoff, K.**, **Schaller, M. and Feil, R.**, Transdifferentiation of vascular smooth muscle cells to macrophage-like cells during atherogenesis. *Circ. Res.* 2014. **115**: 662–667.

36 **Anderson, K. L.**, **Smith, K. A.**, **Perkin, H.**, **Hermanson, G.**, **Anderson, C. G.**, **Jolly, D. J.**, **Maki, R. A. et al.**, PU.1 and the granulocyte- and macrophage colony-stimulating factor receptors play distinct roles in late-stage myeloid cell differentiation. *Blood* 1999. **94**: 2310–2318.

37 **DeKoter, R. P.**, **Walsh, J. C. and Singh, H.**, PU.1 regulates both cytokine-dependent proliferation and differentiation of granulocyte/macrophage progenitors. *EMBO J.* 1998. **17**: 4456–4468.

38 **McKercher, S. R.**, **Henkel, G. W. and Maki, R. A.**, The transcription factor PU.1 does not regulate lineage commitment but has lineage-specific effects. *J. Leukocyte Biol.* 1999. **66**: 727–732.

39 **Wu, Y. and Madri, J.**, Insights into monocyte-driven osteoclastogenesis and its link with hematopoiesis: regulatory roles of PECAM-1 (CD31) and SHP-1. *Crit. Rev. Immunol.* 2010. **30**: 423–433.

40 **Winkler, I. G.**, **Sims, N. A.**, **Pettit, A. R.**, **Barbier, V.**, **Nowlan, B.**, **Helwani, F. Poulton, I. J. et al.**, Bone marrow macrophages maintain hematopoietic stem cell (HSC) niches and their depletion mobilizes HSCs. *Blood* 2010. **116**: 4815–4828.

41 **Saha, P. and Geissmann, F.**, Toward a functional characterization of blood monocytes. *Immunol. Cell Biol.* 2011. **89**: 2–4.

42 **Robbins, C. S.**, **Chudnovskiy, A.**, **Rauch, P. J.**, **Figueiredo, J. L.**, **Iwamoto, Y.**, **Gorbatov, R.**, **Etzrodt, M. et al.**, Extramedullary hematopoiesis generates Ly-6C(high) monocytes that infiltrate atherosclerotic lesions. *Circulation* 2012. **125**: 364–374.

43 **Swirski, F. K.**, **Nahrendorf, M.**, **Etzrodt, M.**, **Wildgruber, M.**, **Cortez-Retamozo, V.**, **Panizzi, P.**, **Figueiredo, J. L. et al.**, Identification of splenic reservoir monocytes and their deployment to inflammatory sites. *Science* 2009. **325**: 612–616.

44 **Ruder, A. V.**, **Wetzels, S. M. W.**, **Temmerman, L. and Biessen, E. A. L.**, Goossens P. Monocyte heterogeneity in cardiovascular disease. *Cardiovasc. Res.* 2023. **119**: 2033–2045.

45 **Yadav, S.**, **Priya, A. and Borade, D. R.**, Agrawal-Rajput R. Macrophage subsets and their role: co-relation with colony-stimulating factor-1 receptor and clinical relevance. *Immunol. Res.* 2023. **71**: 130–152.

46 **Zernecke, A.**, **Erhard, F.**, **Weinberger, T.**, **Schulz, C.**, **Ley, K.**, **Saliba, A. E. and Cochain C.**, Integrated single-cell analysis-based classification of vascular mononuclear phagocytes in mouse and human atherosclerosis. *Cardiovasc. Res.* 2023. **119**: 1676–1689.

Abbreviations: **CSF1R**: colony-stimulating factor 1 · **IPH**: presenting intraplaque hemorrhage · **MaFIA**: macrophage Fas-induced apoptosis · **M-CSF**: macrophage colony-stimulating factor · **SMC**: smooth muscle cells · **TUNEL**: terminal deoxytransferase dUTP nick-end labeling · **vSMC**: vascular smooth muscle cells

Full correspondence: Prof. Erik A.L. Biessen, Dept. of Pathology, Cardiovascular Research Institute Maastricht (CARIM), Maastricht University, 6229 ER Maastricht, the Netherlands
e-mail: erik.biessen@mumc.nl

Received: 21/3/2024
Revised: 29/7/2024
Accepted: 30/7/2024
Accepted article online: 5/8/2024